Zhixin Xiong
Xinyuan Wu ✉
Yu Guo
Ming Ma
Zheng Fu

https://doi.org/10.21278/TOF.482057323
ISSN 1333-1124
eISSN 1849-1391

ANALYSIS OF TRAWL NET FISHING OF ANTARCTIC KRILL IN A POLAR ICE AREA

Summary

To analyse the operations of Antarctic krill fishing vessels in regions with polar ice floes, this study used Star-CCM+ software to simulate the effects of towing speed on the height and width of the midwater trawl net of these vessels. The simulation accorded with the experimental results of Su (2017) and was thus shown to be accurate. The fluctuations in the area of the net and the flow passing through it were determined under different *L*/*S* ratios (the ratio of the horizontal and vertical distances between the ends of the net gear), ice concentrations, and towing speeds. On the basis of the obtained results, a suitable *L*/*S* ratio and towing speed were identified for maximising the fishing efficiency of Antarctic krill fishing vessels. The significant innovation of this article is to link polar ice floes with krill fishing efficiency through net flow. Net flow can more intuitively reflect krill fishing efficiency compared to the net mouth area. Based on the habitat characteristics of Antarctic krill, the conclusion was drawn to choose a trawl with an *L*/*S* ratio of 0.55.

Key words: *Antarctic krill fishing ships, model testing, fishing operations, midwater trawl net*

1. Introduction

Antarctic krill is a key species of the Southern Ocean ecosystem because of its central position in the food web [1,2]. Antarctic krill has an estimated biomass of approximately 300 million tonnes [3], which is the largest known stock of metazoans worldwide. This species remains one of the largest underexploited metazoan stocks in the world [4,5].

With dwindling fishery resources around the globe, the increased value of Antarctic krill, and the maturing of krill processing technology, the considerable potential of Antarctic krill as a resource and its crucial position in the Antarctic ecosystem have begun to be recognised by various countries. The sustainable, efficient, and reasonable development of Antarctic krill resources has received considerable research attention [6].

Antarctic krill mainly inhabit the middle layer or surface layer of the ocean, move vertically during the day and night, and exhibit intense swarming behaviour and weak swimming ability. The midwater trawl net is the main fishing gear for harvesting Antarctic krill because this is a small mesopelagic species that swims slowly [7,8]. A numerical model of midwater trawl net fishing was constructed in the present study.

In general, the net position, net state, and net gear structure are the key factors that determine trawling efficiency [9]. In addition to the net position, the trawl net body is used as a fish guide area, and the quality of the net directly affects the contact between the fishing object and the net, which in turn affects the trawl selectivity and catch quality [10]. The overall state of the trawling net has a crucial influence on operation safety, and the factors affecting the state of the trawling operation are the length of the trawling line, towing speed, wind speed, wave height, and water velocity [11]. In addition, the net structure affects the net gear performance. The main net structure parameters include the body circumference ratio, the length of the net sleeve, and the ratio of the widths of the back (abdominal) net and the side net [12,13].

Since the 1990s, numerical simulation has been used to investigate the performance of trawl net gear. Because numerical simulation can be used to intuitively represent the geometric shape and tension of various parts of the trawl net during operation, this method has gradually become a crucial method for optimising the trawl net's shape and the net gear's performance. A trawl net is made of soft mesh, which is highly flexible; it is affected by water resistance during the hauling process; and it has a specific shape. Computer-based numerical simulation has unique advantages in capturing these sources of complexity in the behaviour of trawl nets. Hu et al. [14] performed a computer simulation on the position control of midwater trawl nets, and their simulation results fit well with their experimental results. Cha et al. [15] developed a physical model based on the spring–mass system and simulated the relationships between towing speed, length of the towing line, and net gear parameters such as net position and net shape. They then compared their simulation results with measurements performed at sea. Takagi et al. [16-18] considered the influence of nodules, converted the foot into two springs, and established a physical model. This model can express the bending of the foot of the eye, and develop the analysis software-NaLA of the net shape and load. Lee et al. [19] used a mesh grouping method to reduce calculations, established a Newtonian mechanics equation, and obtained the model. These authors established a simulation system that can be applied to trawls and seines. Priour et al. [20-22] optimised this system on the basis of sea survey data by accounting for the uneven distribution of fish stocks and the effect of the catch on the trawl system. Sun et al. [23] investigated the influence of the type of trawler on the behaviour of the net gear. Truong et al. [24] used the DynaMIT system to develop a model, compared the results obtained using this model with measurements performed at sea, and determined the strengths and limitations of three methods. Wan et al. used the finite-element method and the principle of minimum potential energy to determine the equilibrium configuration and tension distribution for a trawl net in a uniform current [25]. In a previous study, on the basis of simulated results, suggestions were provided for the dimensions of each component of a trawl system [26]. A 1/35-scale trawl model based on a modified version of Tauti's law was designed by Bruno [27] for Antarctic krill fisheries. This model was tested in a flume tank and the effects were examined of flow velocity, horizontal spread ratio, sinking force, and the ratio of buoyancy to the fishing line weight on a trawl system's engineering performance.

Ships working in polar regions will be subject to environmental tests such as low temperatures, sea ice obstruction, iceberg attacks, and snowstorm attacks. The impact of floating ice is very important for ship operations in the Arctic region. Because Antarctic krill fishing vessels operate in polar regions, they often encounter floating ice. The presence of floating ice and other environmental conditions can affect the speed of fishing ships and thus the operation of trawl nets. However, few studies have investigated the influence of floating ice on the operation of fishing vessels. Therefore, the present study analyses the influence of floating ice on the operation of midwater trawl nets for Antarctic krill fishing. Practical experience indicates that during the trawling process, the mouth of the net is aimed and fully expanded at the centre of the target fish species for a suitable flow state to be achieved for the mouth, which is crucial for achieving high harvest efficiency in fishing operations. In the

present study, the Star-CCM+ software program was used to investigate the performance of trawl net gear under different ratios of the horizontal and vertical distances between the ends of the net gear (*L*/*S*). The mouth area of and flow conditions for the trawl net in an area with floating ice were analysed to optimise the shape of the mouth of the net. The accuracy of the simulation results was determined by comparing them with the experimental results of Su. It is hoped that the results of this study will aid future developments in Antarctic krill fishing.

2. Numerical method

The deformation of a trawl net in seawater depends on how the seawater interacts with the net. This interaction is governed by the laws of the conservation of energy, mass, and momentum. These laws are described in the following sections.

2.1 Basic conservation equations of fluid mechanics

(1) *Mass conservation equation*

Fluid movement is governed by the law of the conservation of mass. This law is expressed as follows [28,29]:

$$\frac{\partial \rho}{\partial t}+\frac{\partial(\rho u)}{\partial x}+\frac{\partial(\rho v)}{\partial y}+\frac{\partial(\rho w)}{\partial z}=0 \tag{1}$$

where ρ is the fluid density at time t, and u, v, and w are the velocity components of a point in space in the x-direction, y-direction, and z-direction, respectively. The aforementioned equation is applicable to compressible flow.

For an incompressible fluid, the fluid density does not change with time; thus, the continuity equation can be expressed as follows:

$$\frac{\partial u}{\partial x}+\frac{\partial v}{\partial y}+\frac{\partial w}{\partial z}=0 \tag{2}$$

The mass conservation equation is a continuous function.

(2) *Momentum conservation equation*

In fluid mechanics, the momentum conservation equation indicates that the vector sum of the forces acting on a finite element in space is equal to the derivative of fluid momentum over time. This equation is expressed as follows:

$$\begin{aligned}
&\frac{\partial(\rho u)}{\partial t}+\nabla\cdot(\rho u v)=-\frac{\partial p}{\partial x}+\frac{\partial \tau_{xx}}{\partial x}+\frac{\partial \tau_{yx}}{\partial y}+\frac{\partial \tau_{zx}}{\partial z}+\rho f_x\\
&\frac{\partial(\rho v)}{\partial t}+\nabla\cdot(\rho v V)=-\frac{\partial p}{\partial y}+\frac{\partial \tau_{xy}}{\partial x}+\frac{\partial \tau_{yy}}{\partial y}+\frac{\partial \tau_{zy}}{\partial z}+\rho f_y\\
&\frac{\partial(\rho w)}{\partial t}+\nabla\cdot(\rho w V)=-\frac{\partial p}{\partial z}+\frac{\partial \tau_{zx}}{\partial x}+\frac{\partial \tau_{zy}}{\partial y}+\frac{\partial \tau_{zz}}{\partial z}+\rho f_z
\end{aligned} \tag{3}$$

where $V = (u, v, w)$ represents the momentum conservation equations in the x-direction, y-direction, and z-directions; f denotes the volume force acting on the microelement, τ is the stress tensor, and p is the pressure acting on the microelement.

2.2 Numerical simulation theory and method of solid mechanics

On the basis of Newton's second law, the finite-element method based on the structural vibration equation involves discretising a solid elastic body into multiple finite elements [30]. After the solid structure is discretised, its mechanical model can be described using the following formula:

$$[K]\{\Delta\}=\{R\} \tag{4}$$

where $\{R\ (t)\}$ denotes the variation in node force over time. The change in the dynamic load over time can be expressed as follows:

$$\{R(t)\} = \{F(t)\} + \{P_T(t)\} + \{P_C(t)\} \tag{5}$$

where $[M]$ And $[C]$ denote the mass matrix and damping matrix, respectively, and $\{\dot{\Delta}t\}$ and $\{\ddot{\Delta}t\}$ denote the acceleration matrix and velocity matrix, respectively. The mechanical model of elastic structures can also be represented as follows:

$$[K]\{\Delta\} = \{F(t)\} - [M]\{\ddot{\Delta}(t)\} - [C]\{\dot{\Delta}(t)\} \tag{6}$$

2.3 Numerical simulation theory for fluid–structure interactions

Finite-element analysis and computational fluid dynamics, which are used for analysing solid and liquid systems, respectively, are mature simulation methods. However, analysing a system with fluid and solids is difficult for the following reasons: (1) the different coordinate systems used for analysing solids and fluids; (2) the incompatibility between the Lagrange and Euler methods, which are used for analysing solids and fluids, respectively; and (3) the difficulty in determining the parameters of the solid and fluid domains at their interface. The Lagrangian and Eulerian coordinate systems are used for describing the motion of particles in solid mechanics and the spatial state of fluid parcels in fluid mechanics, respectively. In the Lagrange method, mesh nodes coincide with the particles of a solid object and deform and move with the deformation of the object; no relative motion occurs between the solid and the mesh. The Lagrange method can be used to accurately and elegantly describe the node motion on a coupled surface. When large-deformation problems are encountered in the Lagrange method, the deformation of the solid structure causes mesh distortion, which results in a considerable decrease in computational accuracy and even the termination of the calculation. In the Euler method, the mesh is fixed in a specific space and is unaffected by the deformation and motion of solids; thus, this method can be used for easily solving various solid-deformation problems. However, in the Euler method, relative motion occurs between the grid and the solid (called convective motion), which can lead to oscillatory solutions for finite-element equations.

The arbitrary Lagrange–Euler (ALE) method combines the advantages of Lagrange and Euler descriptions. This method not only enables the accurate tracking of the motion and deformation of a solid but also allows the spatial grid and solid to exist separately. When a solution is being computed, the grid can automatically adjust its position and deformation, thereby effectively describing the motion trajectory of particles on a coupling interface. The ALE method can also solve the problem of the large deformation of solid structures. In the ALE method, two sets of overlapping grids are used, and data are transmitted in these grids through nodes [31].

The ALE hydrodynamic equation is derived from its Eulerian counterpart; the only difference between these equations is that the time derivative of the material quantity is considered in the equation of the ALE method.

The time derivative of the material quantity is expressed as follows:

$$\frac{\mathrm{d}f}{\mathrm{d}t} = f_{t[x]} + c \cdot \nabla_x f \tag{7}$$

where ∇x represents the spatial gradient.

(1) *Mass conservation equation*

The mass conservation equation is expressed as follows:

$$\rho_{t[x]} + c \cdot \nabla_x \rho + \rho \nabla_x \cdot v = 0 \tag{8}$$

where c is the convective velocity and v is the material velocity. When the fluid is incompressible, the aforementioned equation can be simplified as follows:

$$\nabla_x \cdot v = 0 \tag{9}$$

(2) *Momentum conservation equation*

The momentum conservation equation is expressed as follows:

$$\mathrm{P}(v_{t[x]} + (c \cdot \nabla_x)v) = \nabla_x \cdot \sigma + \rho b \tag{10}$$

where b is the physical force vector per unit mass and σ is the stress tensor.

(3) *Energy conservation equation*

The energy conservation equation is expressed as follows:

$$\mathrm{P}(e_{t[x]} + (c \cdot \nabla_x)e) = D : \sigma + \nabla_x \cdot q - \rho s \tag{11}$$

where e is the internal energy per unit mass, q is the heat flux vector per unit area, ρS is the heat per unit volume, and D is the deformation rate. If the heat exchange rate is assumed to be negligible, the energy conservation equation can be ignored, and only the first two equations must be solved.

3. Settings of the net gear model

A model of the midwater trawl net used in Chinese Antarctic krill fishing ships was developed and used in the numerical simulations of this study. The scale ratio of this model was 1:35. The Star-CCM+ software program was used to conduct the numerical simulations.

Because the trawl was symmetric, a semicircular fluid area was created, and half the geometric model was analysed (Figure 2). The trawl selects the solid stress and Rayleigh damping in the physical model, and the fluid selects the k-ε turbulence model. To divide the grid, the basic size of the grid was set at 0.01 m. A fluid–structure interface was also created by establishing contact between the fluid and the mesh. In fluid–structure interaction problems, the fluid and solid domains can exchange data at their interface. The displacement and resistance of the net gear were simulated, as illustrated in Figure 1.

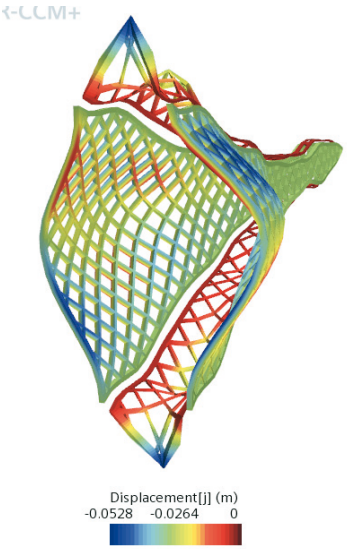

Fig. 1 Displacement of the floating trawl

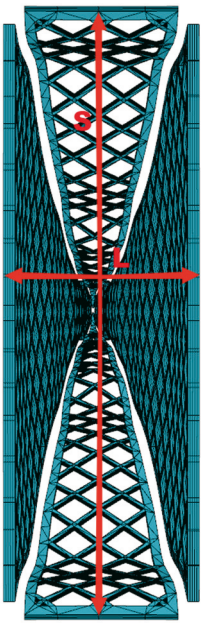

Fig. 2 Horizontal spacing L and vertical spacing S between the ends of the net gear

The shape of the net mouth was determined in terms of the ratio of the horizontal and vertical distances (L and S, respectively) between the ends of the net gear (Figure 2).

The L/S ratios in the simulations were 0.35, 0.40, 0.45, 0.50, and 0.55. Five simulations were performed for each L/S ratio. The L/S settings are presented in Table 1, and the towing speeds of a full-scale ship and the developed scaled model are presented in Table 2.

Table 1 L/S settings in the simulations

L/S	Length of ground rope S /m	Horizontal spacing L /m
0.35	58.1	20.3
0.40	58.1	23.1
0.45	58.1	26.3
0.50	58.1	29.1
0.55	58.1	31.85

Table 2 Towing speeds (kn) of a full-scale ship and the developed scaled model

Full scale ship	1.5	2.0	2.5	3	3.5
Scaled model	0.2837	0.3782	0.3782	0.5674	0.6619

4. Analysis of net gear performance

The relationships of the width and height of the net mouth with the towing speed were simulated under different L/S values (Figures 3 and 4, respectively). Figure 3 indicates that the width of the net mouth increased with the towing speed under different L/S ratios. However, Figure 4 indicates that the height of the net mouth decreased with an increase in the towing speed under different L/S ratios. The width and height of the net mouth increased and decreased with an increase in the L/S ratio, respectively.

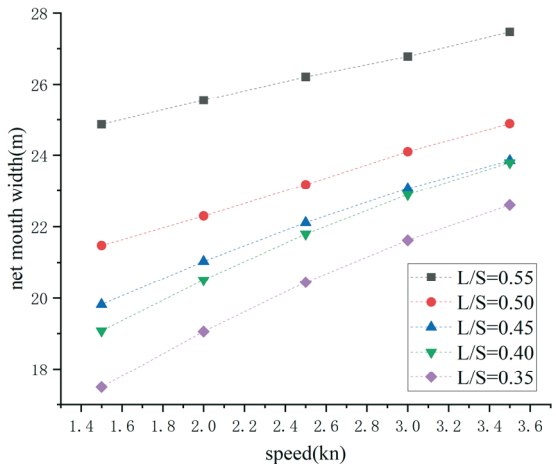

Fig. 3 Variations in the width of the net mouth with the towing speed under different L/S values

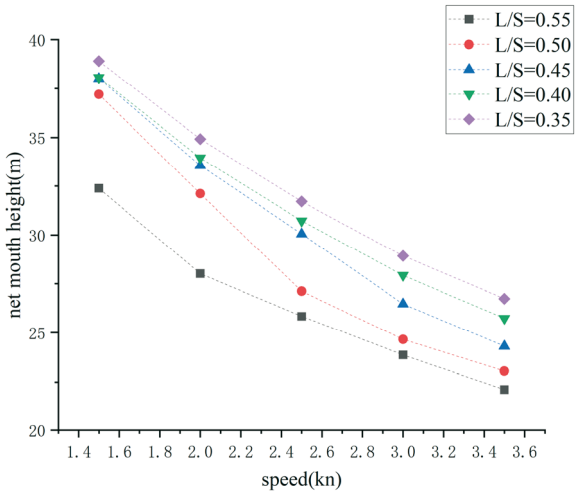

Fig. 4 Variations in the height of the net mouth with the towing speed under different L/S values

5. Comparison between the simulation results and experimental results

To determine the accuracy of the simulations, the simulation results of this study were compared against the experimental results of Su, who developed a trawl net and tested it in a hydrodynamic circulating tank in Tokyo Ocean University, Japan [32]. The test trawl had a scale ratio of 1:35, and the L/S ratios in the experiment were consistent with those in the simulations of the present study. The experimental testing of the trawl model is illustrated in Figure 5.

Fig. 5 Experimental test of the trawl model by Su (Source: Su Zhi Peng)

Figures 6 and 7 display the experimental and numerical variations in the width and height of the net mouth, respectively, with the towing speed under different *L*/*S* ratios.

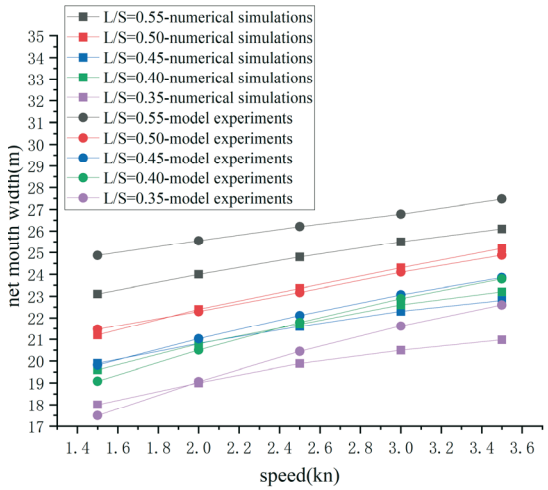

Fig. 6 Experimental and numerical variations in the width of the net mouth with towing speed under different *L*/*S* ratios

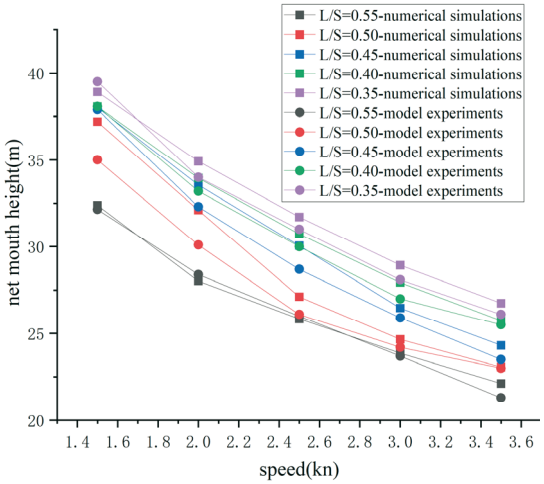

Fig. 7 Experimental and numerical variations in the height of the net mouth with towing speed under different *L*/*S* ratios

The results displayed in Figures 6 and 7 indicate that the experimental and numerical results were consistent; thus, the simulated results were accurate. The maximum errors of 7.4% and 7.6% were observed for an *L*/*S* ratio of 0.55 and a towing speed of 1.5 kn.

6. Net mouth area

When a net gear moves in water, the mouth of the net can be considered to have an elliptical shape. At any given circumference, ellipses that more closely approximate a circle have a larger area. Moreover, a larger net mouth area is more favourable during trawling operations. Therefore, the shape and area of the net are parameters that can best reflect the performance of the net gear. Figure 8 depicts the shape of the net mouth under different *L*/*S* ratios and towing speeds (the long and short axes represent the height and width of the net mouth, respectively). When the towing speed was 1.5, 2.0, or 2.5 kn, the optimal *L*/*S* ratio was 0.55. When the towing speed was 3 or 3.5 kn, the optimal *L*/*S* ratio was 0.40. Figure 9 indicates that the area of the net mouth gradually decreased with the towing speed. Thus, when the net expanded horizontally, the effects of the towing speed on the height and width of the net mouth

were inconsistent. At high towing speeds, the rate of decrease in the height of the net mouth with the towing speed was greater than the rate of increase in the width of the net mouth with the towing speed.

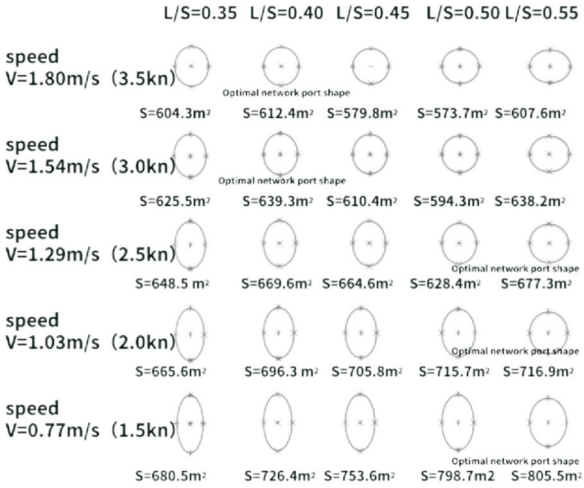

Fig. 8 Shape of the net mouth under different *L*/*S* ratios and towing speed

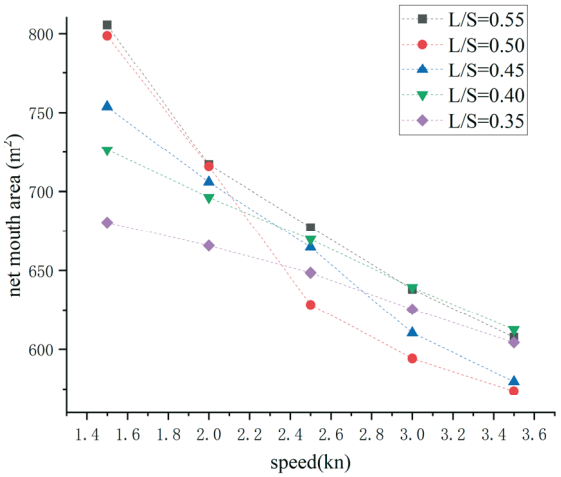

Fig. 9 Variation in the area of the net mouth with towing speed under different *L*/*S* values

7. Variations in the area and flow of the net mouth under different amounts of floating ice

The starting point of the selected simulation route is Taicang Port, and the destination is Rotterdam, the Netherlands. The polar route starts from Taicang Port, passing through Busan Port, Bering Strait, the North Sea Route, Norway North Sea to Rotterdam, the Netherlands. The selected voyage distances for each segment are shown in Table 3.

In practical fishing operations, the speed of an Antarctic krill fishing ship corresponds to the towing speed of the midwater trawl net used by the ship. When a ship is sailing at a fixed speed, the towing speed is not fixed but varies around a specified speed. Because Antarctic krill fishing ships generally operate in regions with polar ice floes, the speed data for relevant regions [6] must be used to establish a towing speed fluctuation map for different ice floe densities (Figure 10).

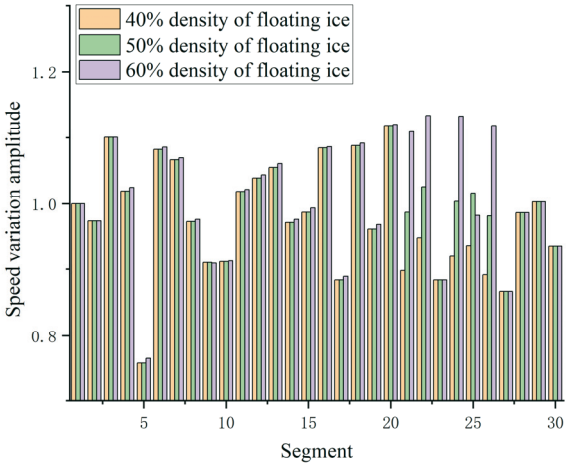

Fig. 10 Variations in towing speed in different segments

Table 3 Segment settings for fishing operations

Segment number	Range（nmile）	wind direction	wind scale
1	9.79	headwind	3
2	308.4	headwind	4
3	99.78	headwind	4
4	185.22	crosswind	4
5	647.9	downwind	4
6	49.39	headwind	4
7	64.36	headwind	4
8	621.08	downwind	4
9	312.55	downwind	5
10	353.51	downwind	4
11	276.96	downwind	6
12	69.1	headwind	5
13	218.23	headwind	3
14	56.16	downwind	4
15	118.79	downwind	4
16	10.24	headwind	4
17	69.23	downwind	3
18	110.16	headwind	4
19	184.86	downwind	5
20	120.32	headwind	4
21	429.35	headwind	4
22	204.91	headwind	2
23	442.67	downwind	4
24	11.88	headwind	3
25	171.57	headwind	3
26	43.14	headwind	3
27	906.56	downwind	4
28	567.14	downwind	3
29	278.9	downwind	3
30	662.74	downwind	3

On the basis of Figures 9 and 10, the variations in the area of the net mouth were determined under a specific ship speed, ice concentration, and L/S ratio. Figures 11–13 depict the fluctuations in the area of the net mouth at vessel speeds of 2, 2.5, and 3 kn, respectively, under ice concentrations of 40%, 50%, and 60%, as well as different L/S ratios.

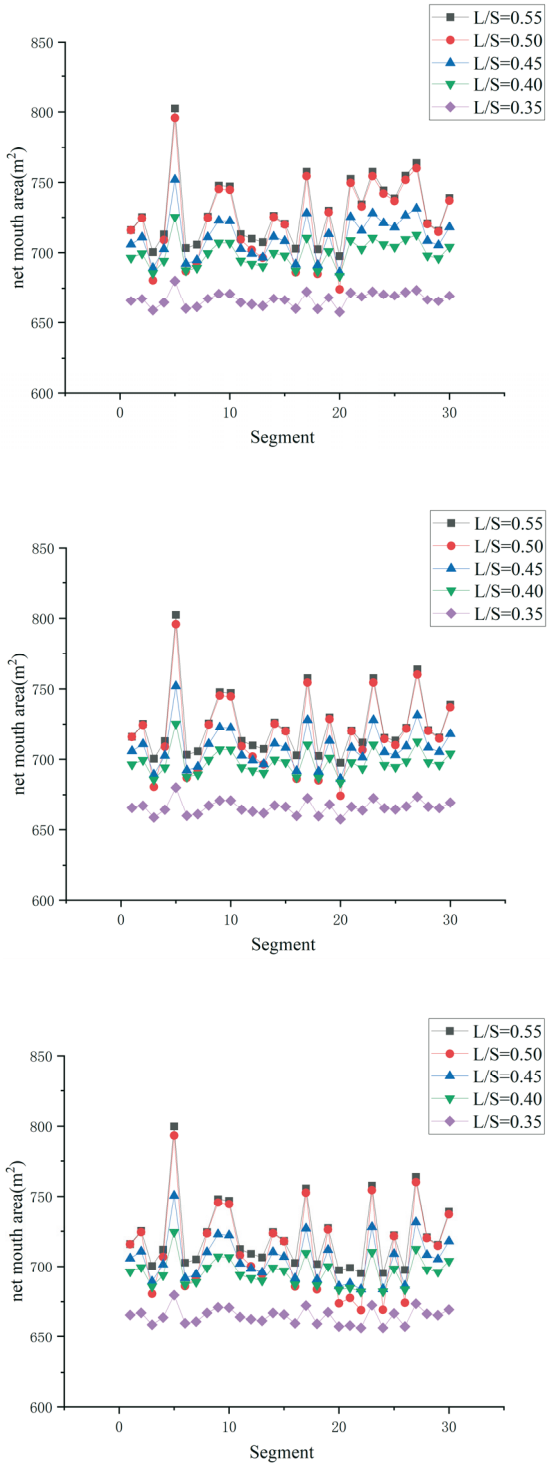

Fig. 11 Variations in the area of the net mouth under a ship speed of 2 kn under different *L*/*S* ratios and ice concentrations of 40%, 50%, and 60%

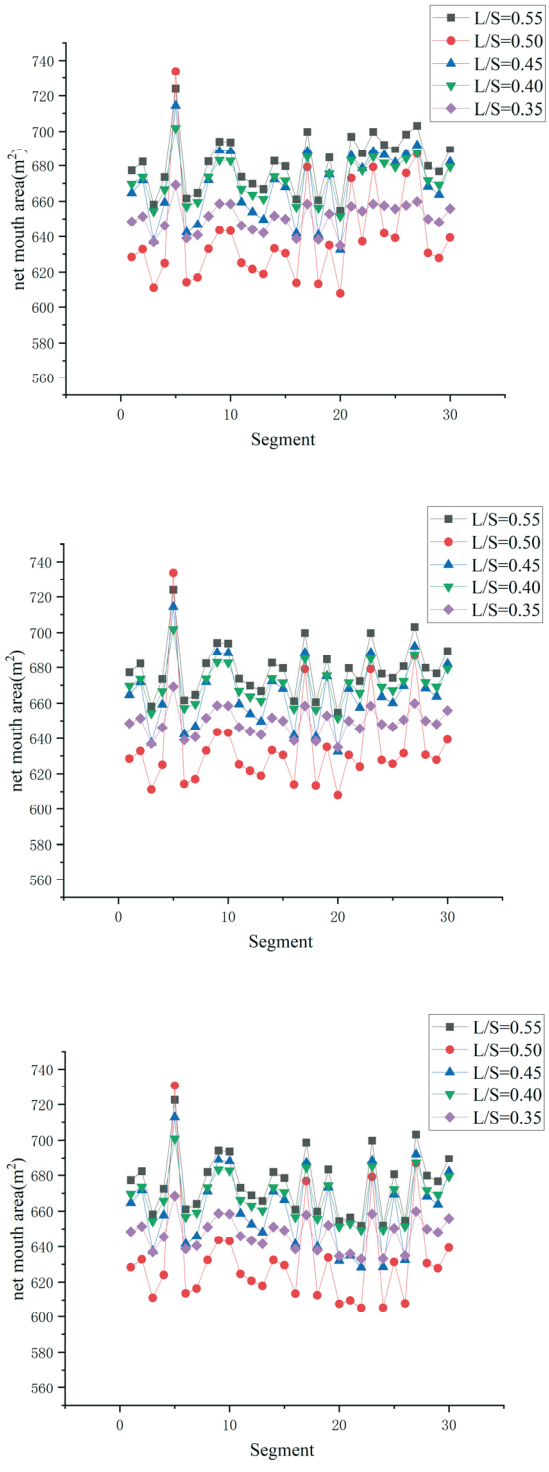

Fig. 12 Variations in the area of the net mouth under a ship speed of 2.5 kn under different *L*/*S* ratios and ice concentrations of 40%, 50%, and 60%

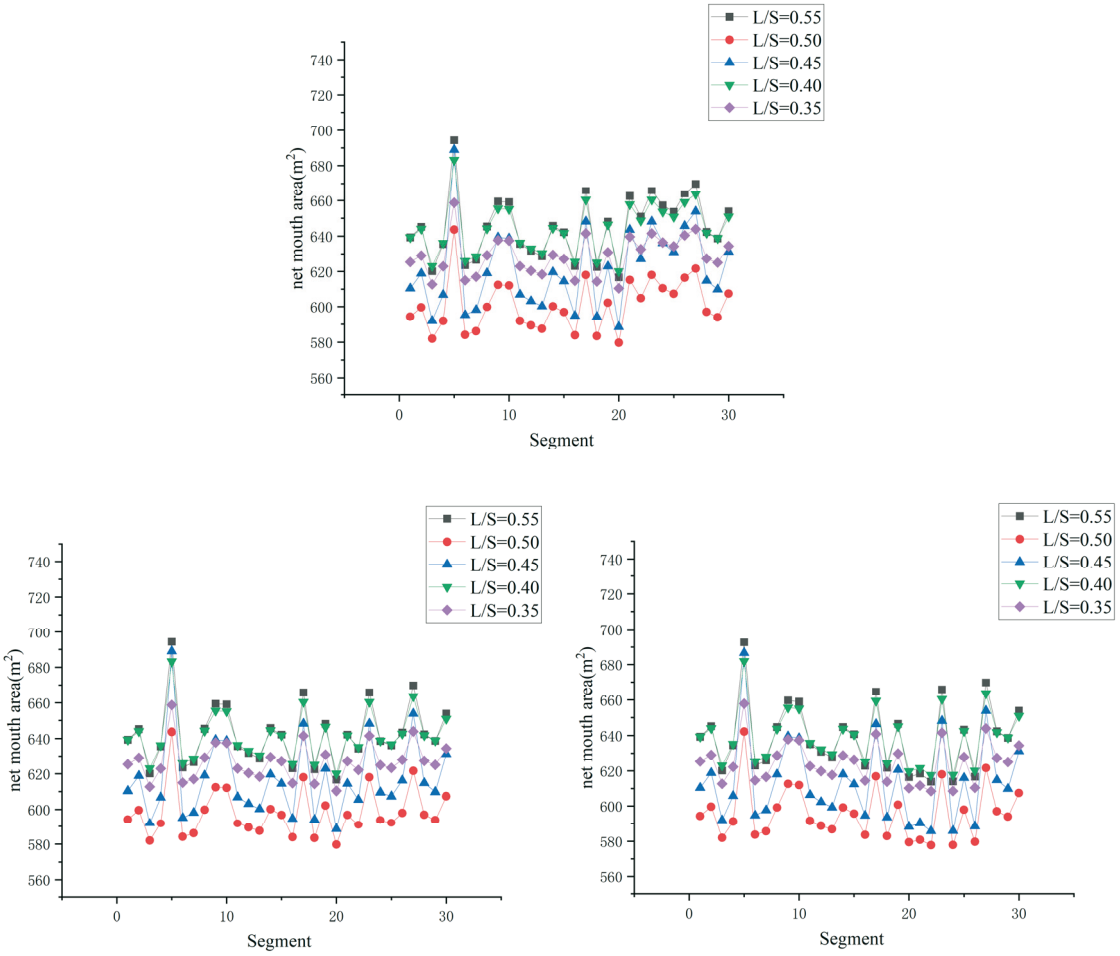

Fig. 13 Variations in the area of the net mouth under a ship speed of 3 kn under different *L*/*S* ratios and ice concentrations of 40%, 50%, and 60%

Thus, 45 curves of the variations in the area of the net mouth were obtained from the 15 data points in the original graph of the area of the net mouth versus the vessel speed. These 45 curves provide a comprehensive and intuitive view of the variations in the area of the net mouth under different *L*/*S* ratios and ice concentrations.

Because voyage distance and vessel speed differ between the legs of a voyage, the area of the net mouth alone cannot provide a clear representation of the fishing efficiency of Antarctic krill fishing vessels. Therefore, on the basis of the voyage distances presented in Table 3, the volume flowing through the net mouth during each leg was determined. Subsequently, 45 curves were obtained of the variations in the aforementioned volume with the ice floe concentration, *L*/*S* ratio, and ship speed (Figures 14–16). The conversion formula is shown in Equation 12.

$$Q_n = \frac{Segment_n \cdot area_n}{t_n} \tag{12}$$

where Q_n represents the flow rate of the *n*th segment, $Segment_n$ represents the distance of the *n*th segment, $area_n$ represents the net mouth area when passing through the *n*th segment, and t_n represents the time required to pass through the *n*th segment.

These curves are displayed in Figures 14-16. Because the amount of net flow represents the volume of fluid swept by the trawl during a specific time, it can directly reflect the fishing efficiency of Antarctic krill vessels.

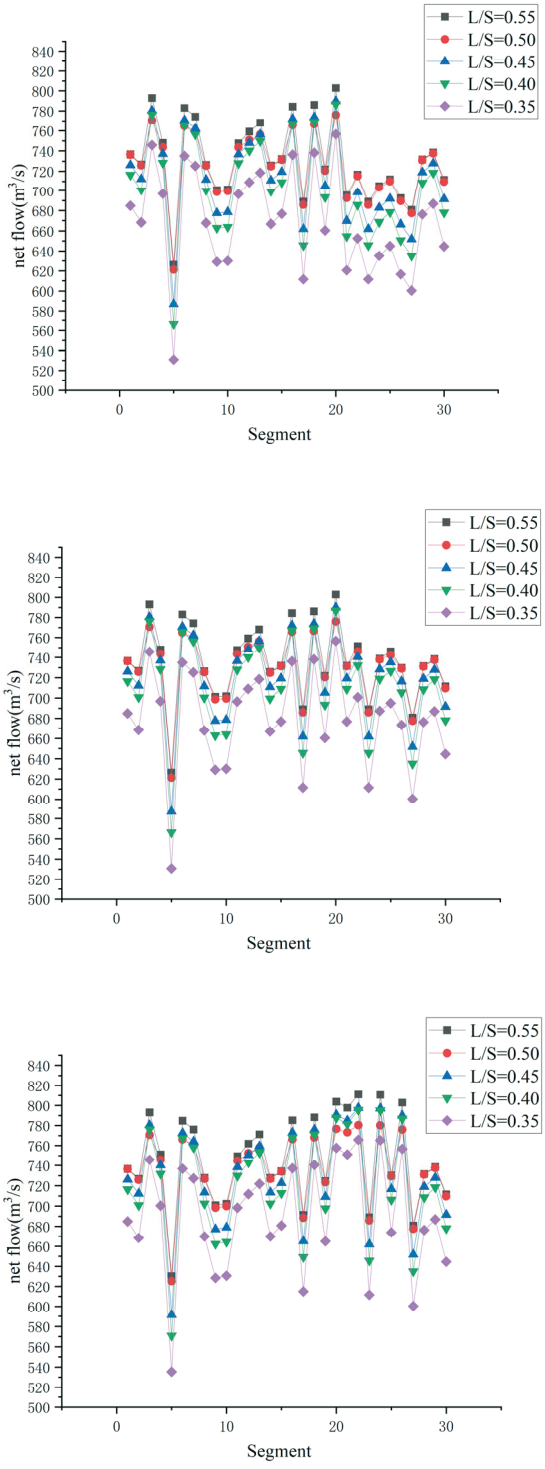

Fig. 14 Variations in flow passing through the net mouth area under a ship speed of 2 kn under different *L*/*S* ratios and ice concentrations of 40%, 50%, and 60%

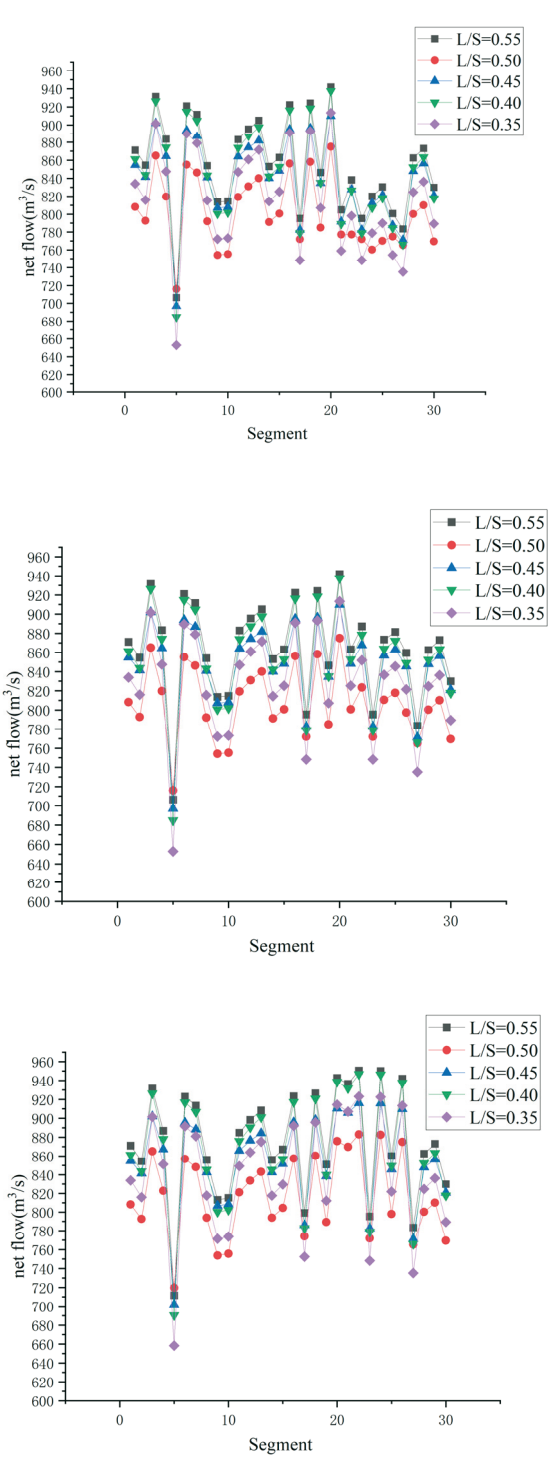

Fig. 15 Variations in flow passing through the net mouth area under a ship speed of 2.5 kn under different *L*/*S* ratios and ice concentrations of 40%, 50%, and 60%

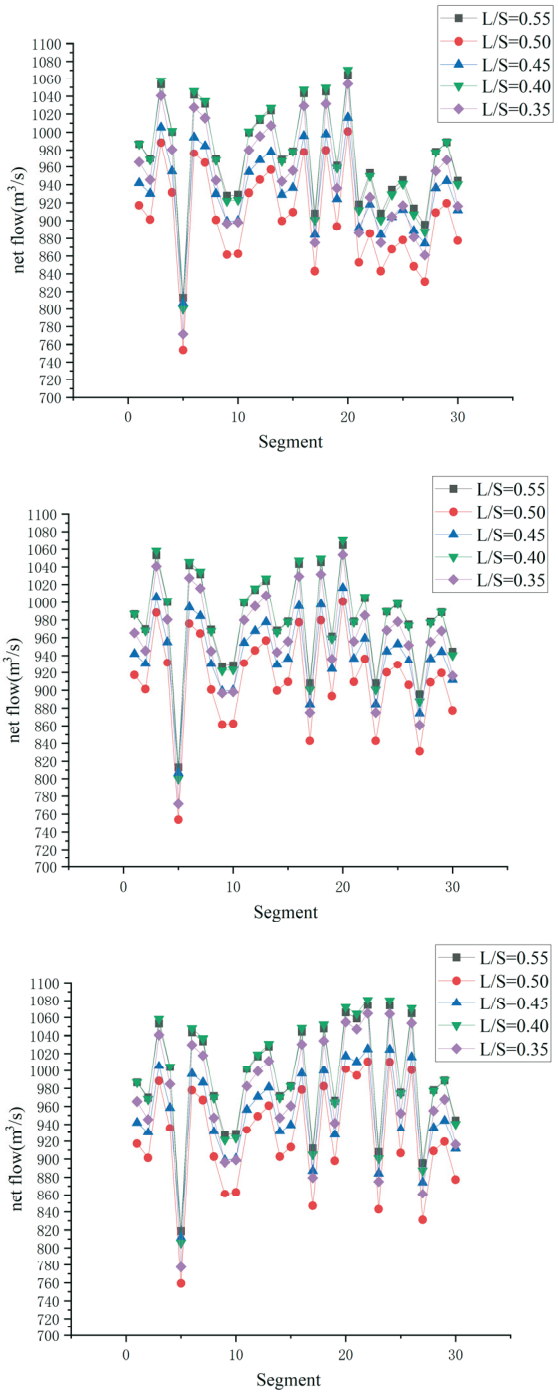

Fig. 16 Variations in flow passing through the net mouth area under a ship speed of 3 kn under different *L*/*S* ratios and ice concentrations of 40%, 50%, and 60%

Although the area of the net mouth was inversely proportional to the ship speed, the overall flow passing through the net was directly proportional to the ship speed. Moreover, under the same ship speed, an increase in the ice concentration resulted in an increase in the flow through the net. This result can be explained by the fact that ships move much faster at higher ice concentrations to ensure navigation safety, which results in an increase in the flow through the net.

Research [7] has indicated that to catch krill from the surface layer, the net is typically set at a depth of 5–15 m, and the recommended towing speed is approximately 1.8–2.5 kn. To catch krill from deeper layers, the net is typically set at a depth of approximately 200 m, and the

towing speed is approximately 2.5 ± 0.5 kn. According to Figure 15, to maximise the efficiency of the operations of Antarctic krill fishing vessels, nets with an *L*/*S* ratio of 0.55 should be used.

8. Conclusion

This study numerically simulated the towing of the midwater trawling gear of an Antarctic krill fishing ship in a polar ice area. The numerical simulations were found to be accurate when compared to the experimental results of Su. The simulation results indicate that the height and width of the net mouth decreased and increased, respectively, at higher towing speeds. Moreover, at higher towing speeds, the rate of decrease in the height of the net mouth with towing speed was greater than the rate of increase in the width of the net mouth with towing speed.

The results indicate that the optimal *L*/*S* ratio at towing speeds of 1.5, 2.0, and 2.5 kn is 0.55. However, at towing speeds of 3.0 and 3.5 kn, the optimal *L*/*S* ratio is 0.40.

Due to the fact that Antarctic krill fishing vessels operate in regions with polar ice floes, considerable variation is observed in their speed. Ship speed data for regions with polar ice floes were investigated to obtain a graph of the fluctuation in ship speed. This graph allowed curves of the fluctuations of the area of the net mouth to be obtained for different ice concentrations. Thus, comprehensive insights were obtained regarding changes in the area of the net mouth throughout the journey of an Antarctic krill fishing ship.

Since the legs of the journey of an Antarctic krill fishing ship differ in terms of distance and average ship speed, the fluctuation curves of the area of the net mouth alone cannot provide a direct visualisation of the fishing efficiency of such a ship. Therefore, fluctuation curves for the flow passing through the net were plotted to represent the fishing efficiency of Antarctic krill fishing ships. Given the habitat of Antarctic krill, the speed of relevant fishing ships is approximately 2.5 ± 0.5 kn. Therefore, a net with an *L*/*S* ratio of 0.55 should be selected to maximise the fishing efficiency of Antarctic krill fishing ships.

REFERENCES

[1] Katharina Michael, Lavinia A. Suberg , Wiebke Wessels , So Kawaguchi , Bettina Meyer. Facing Southern Ocean warming: Temperature effects on whole animal performance of Antarctic krill (Euphausia superba).*Zoology* 146 ,**2021**, 125910. https://doi.org/10.1016/j.zool.2021.125910

[2] McBride, M.M., Stokke, O.S., Renner, A.H., Krafft, B.A., Bergstad, O.A., Biuw, M., Lowther, A.D., Stiansen, J.E., Antarctic krill Euphausia superba: spatial distribution, abundance, and management of fisheries in a changing climate. *Marine ecology progress series*. **2021**.668, 185–214. https://doi.org/10.3354/meps13705

[3] Zhongfeng Zhang, Qingwen Xue, Lixia Wen, Weihua Peng, Han Shao, Wenzhi Fu: Study on Multi-step Forming Paths for Double Curved Parts of 1561 Aluminium Alloy, *Transactions of FAMENA* 2,**2023,**34-44. https://doi.org/10.21278/tof.472051222

[4] Atkinson, A., Siegel, V., Pakhomov, E.A., Jessopp, M.J., Loeb, V.A., Re-appraisal of the total biomass and annual production of Antarctic krill. Deep-Sea Research. *Part I-Oceanographic. Research. Papers.* **2009**.56, 727–740. 727–740. https://doi.org/10.1016/j.dsr.2008.12.007

[5] Nicol, S., Foster, J., Kawaguchi, S., 2012. The fishery for Antarctic krill–recent developments. *Fishes* , **2012**. 13 (1), 30–40. https://doi.org/10.1111/j.1467-2979.2011.00406.x

[6] Rod Cappell, Graeme MacFadyen, Andrew Constable, Research funding and economic aspects of the Antarctic krill fishery. *Marine Policy* 143 ,**2022**, 105200. https://doi.org/10.1016/j.marpol.2022.105200

[7] Nicol, S., Foster, J., 2016. The fishery for Antarctic krill: its current status and management regime. In: Biology and Ecology of Antarctic Krill. Springer International Publishing, *Ppar Research* **2016.** 387-421. https://doi.org/10.1007/978-3-319-29279-3_11

[8] Wan, R., Mingxiu, J., Qinglong, G., Liuyi, H., Hui, Ch, Fenfang, Z., Pingguo, H., Fuxiang, H., 2019. Hydrodynamic performance of a newly-designed Antarctic krill trawl using numerical simulation and physical modeling methods. Ocean Engineering. **2019.** 179, 173-179. https://doi.org/10.1016/j.oceaneng.2019.03.022

[9] Park H.H, Cho B K, Ko G S, et al. The Gear Shape and Cross Section of Sweep at Mouth of a Bottom Trawl[J]. *Journal of the Korean Society of Fisheries and Ocean Technology*, **2008**, 44(2): 120-128. https://doi.org/10.3796/ksft.2008.44.2.120

[10] Martín J, Puig P, Palanques A, et al. Trawling-induced Daily Sediment Resuspension in the Flank of a Mediterranean Submarine Canyon[J]. Deep-sea Research, Part II. *Topical Studies in Oceanography*, **2014,** 104: 174-183. https://doi.org/10.1016/j.dsr2.2013.05.036

[11] Puig P, Canals M, Company J B, et al. Ploughing the Deep Sea Floor[J]. *Nature,* **2012**, 489(7415): 286-289. https://doi.org/10.1038/nature11410

[12] LIU W, TANG H, YOU X X, et al. Effect of cutting ratio and catch on drag performance and fluttering motions of midwater trawl codend[J]. *Journal of Marine Science and Engineering,* **2021**, 9(3): 256. https://doi.org/10.3390/jmse9030256

[13] Priour D. Numerical Optimisation of Trawls Design to Improve Their Energy Efficiency[J]. *Fisheries Research*, **2009**, 98(1): 40-50. https://doi.org/10.1016/j.fishres.2009.03.015.

[14] HU F X, TOKAI T, MATUDA K A computer simulation for the net position control of midwater trawl system[J].*Nippon Suisan Gakkaishi*,**2001**,67(2) : 226 - 230. https://doi.org/10.2331/suisan.67.226

[15] Cha B J, Lee C W. Dynamic simulation of a midwater trawl system's behavior[J]. *Fisheries science*, **2002**, (68): 1865-1868. https://doi.org/10.2331/fishsci.68.sup2_1865

[16] Takagi T, Suzuki K, Hiraishi T. Development of the numerical simulation method of dynamic fishing net shape[J]. *Bulletin of the Japanese Society of Scientific Fisheries (Japan)*, **2002**. https://doi.org/10.2331/suisan.68.320

[17] Takagi T, Suzuki K, Hiraishi T. Modeling of net for calculation method of dynamic fishing net shape[J]. *Fisheries science*, **2002**, (68): 1857-1860. https://doi.org/10.2331/fishsci.68.sup2_1857

[18] Takagi T, Shimizu T, Suzuki K, et al. Validity and layout of ―NaLA: a net configuration and loading analysis system[J]. *Fisheries Research*, **2004**, 66(2): 235-243. https://doi.org/10.1016/s0165-7836(03)00204-2

[19] Lee C W, Lee J H, Cha B J, et al. Physical modeling for underwater flexible systems dynamic simulation[J]. O*cean engineering*, **2005,** 32(4): 331-347. https://doi.org/10.1016/j.oceaneng.2004.08.007.

[20] Priour D. Numerical optimisation of trawls design to improve their energy efficiency[J]. *Fisheries Research*, **2009**, 98(1): 40-50. https://doi.org/10.1016/j.fishres.2009.03.015

[21] Khaled R, Priour D, Billard J Y. Numerical optimization of trawl energy efficiency taking into account fish distribution[J]. *Ocean engineering*, **2012**, 54: 34-45. https://doi.org/10.1016/j.oceaneng.2012.07.014

[22] Jurica Sorić, Matej Stanić, Tomislav Lesičar: On Neural Network Application in Solid Mechanics, *Trans of Famena* 2,**2023,**45-66. https://doi.org/10.21278/tof.472053023

[23] Sun X, Yin Y, Jin Y, et al. The Modelling of single-boat, mid-water trawl systems for fishing simulation[J]. *Fisheries Research*, **2011**, 109(1):7-15. https://doi.org/10.1016/j.fishres.2010.12.027

[24] Nguyen T X, Winger P D, Orr D, et al. Computer simulation and flume tank testing of scale engineering models: How well do these techniques predict full-scale at-sea performance of bottom trawls[J]. *Fisheries Research*, **2015**, 161:217-225. https://doi.org/10.1016/j.fishres.2014.08.007

[25] Rong Wan, Mingxiu Jia, Qinglong Guan etc. Hydrodynamic performance of a newly-designed Antarctic krill trawl using numerical simulation and physical Modelling methods. *Ocean Engineering* 179 ,**2019**,173–179. https://doi.org/10.1016/j.oceaneng.2019.03.022

[26] Rong Wan, Qinglong Guan , Liuyi Huang, etc. Effects of otter board and cable length on hydrodynamic performance of Antarctic krill trawl system. *Ocean Engineering* 236 ,**2021,** 109408. https://doi.org/10.1016/j.oceaneng.2021.109408

[27] Bruno Thierry Nyatchouba Nsangue, Hao Tang, Achille Pandong, Liuxiong Xu. Examining engineering performance of midwater trawl with different horizontal spread ratio, floatage, and weight parameters: A case study of model net for Antarctic krill fisheries. *International Journal of Naval Architecture and Ocean Engineering* 14 ,**2022,** 100448. https://doi.org/10.1016/j.ijnaoe.2022.100448

[28] Georgiev, P., Garbatov, Y. Multipurpose vessel fleet for short black sea shipping through multimodal transport corridors. *Brodogradnja*, **2021**,72(4), 79-101. https://doi.org/10.21278/brod72405

[29] Norozi H. R., Za Rghami R., So T. R. .Couple CFD-DEM Modeling: Formulation, Implementation and Application to Multiphase Flows. *Wiley Online Library,* **2016**,165(2): 752-770.

[30] Norberg, C. Flow around Rectangular Cylinders: Pressure Forces and Wake Frequencies. *Journal of Wind Engineering and Industrial Aerodynamics,* Dec. **1993,** 187–96. https://doi.org/10.1016/0167-6105(93)90014-F

[31] Walton K., The effective elastic moduli of a random packing of spheres. *Journal of The Mechanics And Physi of Solids*,**1987**,35(2) : 213 ~ 226. https://doi.org/10.1016/0022-5096(87)90036-6

[32] Su Zhipeng, Analysis of the performance of Antarctic krill middle layer trawl based on sea measurements and model experiments [D]. *Shanghai Ocean University*, **2017,** 45-66.

Submitted: 17.8.2023

Accepted: 15.01.2024

Zhixin Xiong[1]
Xinyuan Wu[1*]
Yu Guo[2]
Ming Ma[1]
Zheng Fu[1]
[1]College of Ocean Science and Engineering, Shanghai Maritime University, Shanghai, PR China
[2]Marine Design & Research Institute of China, Shanghai, PR China
*Corresponding author: 202130410064@stu.shmtu.edu.cn